Supporting Information

Dual-Targeted Multifunctional Nanoparticles for Magnetic Resonance Imaging Guided Cancer Diagnosis and Therapy

Xueyan Nan,[†] *Xiujuan Zhang,*[*,†] *Yanqiu Liu,*[†] *Mengjiao Zhou,*[†] *Xianfeng Chen,*[*,‡] *and Xiaohong Zhang*[*,†]

[†]Institute of Functional Nano & Soft Materials (FUNSOM) and Jiangsu Key Laboratory for Carbon-Based Functional Materials & Devices, Soochow University, Suzhou Jiangsu, 215123, P. R. China

[‡]Institute for Bioengineering, School of Engineering, University of Edinburgh, Edinburgh EH9 3JL, United Kingdom

* (X. J. Z.) Phone: +86-512-65880955; e-mail: xjzhang@suda.edu.cn.

* (X. H. Z.) Phone: +86-512-65880631; e-mail: xiaohong_zhang@suda.edu.cn.

* (X. C.) Phone: +44-131-6502784; e-mail: xianfeng.chen@oxon.org.

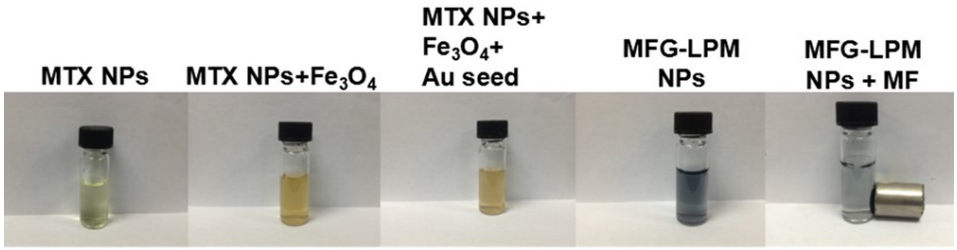

Figure S1. Photographs of MTX NPs, MTX NPs + Fe_3O_4, MTX NPs + Fe_3O_4 + Au seed, MFG-LPM NPs and MFG-LPM NPs + MF.

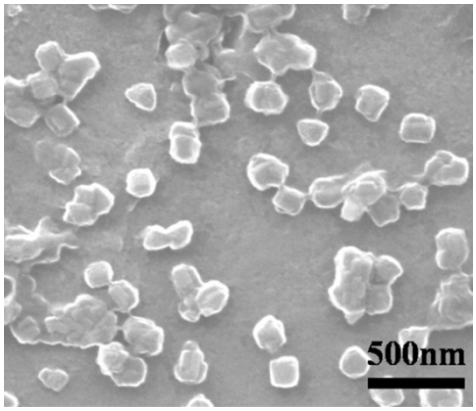

Figure S2. SEM image of MTX NPs.

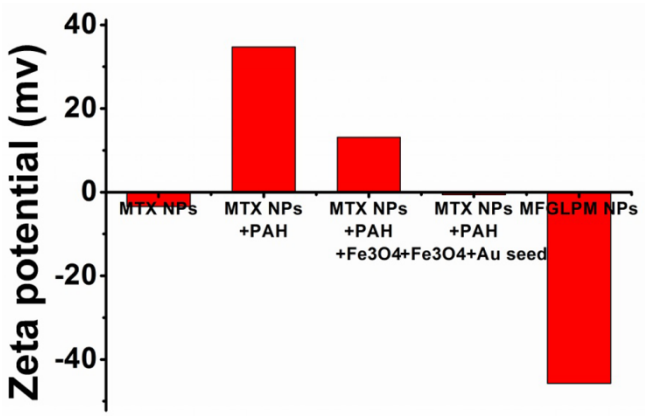

Figure S3. The values of the zeta-potential of nanostructures at different stages during the preparation of MFG-LPM NPs.

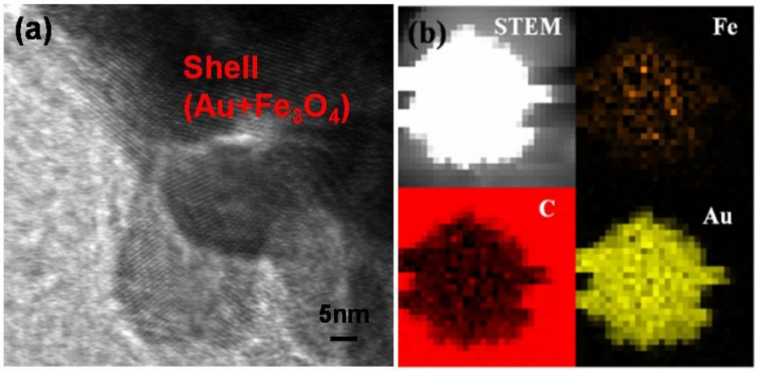

Figure S4. (a) HRTEM image of a thin gold shell and Fe_3O_4 NPs grown on the surface of MTX core NPs. (b) STEM image and HAADF-STEM-EDS mapping images of MFG-LPM NPs.

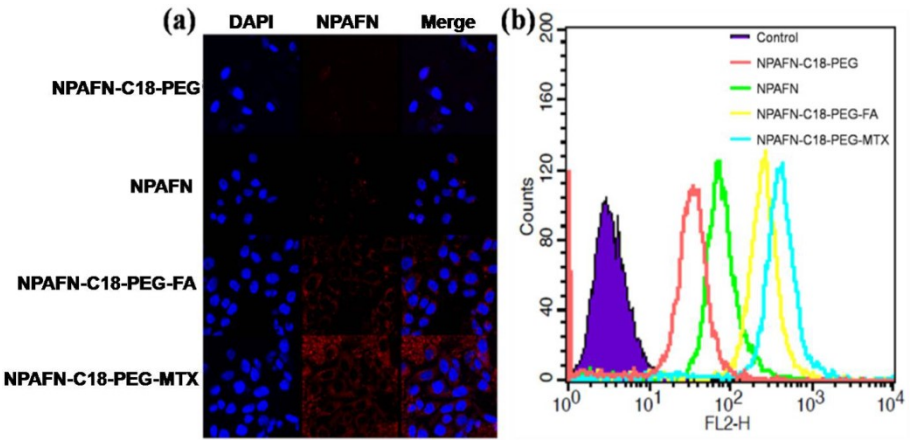

Figure S5. Laser scanning confocal images (a) and flow cytometry results (b) of KB cells after incubation with NPAFN-C18-PEG NPs, NPAFN NPs, NPAFN-C18-PEG-FA NPs and NPAFN-C18-PEG-MTX for 24 h. In the images, the nuclei are stained with DAPI signal in blue and the red fluorescence signal is from NPAFN NPs.

To explore the efficacy of using MTX as the active targeting ligands in our drug delivery system, we conjugated MTX to the surface of fluorescent NPAFN NPs and studied their cellular uptake in human nasopharyngeal epidermal carcinoma (KB) cell line. The KB cells are known to have overexpression of folate receptor-α. Therefore, MTX modified NPAFN NPs should be able to target these cells. In the experiments, KB cells were cultured in FA free medium. The NPs' cellular uptake was measured by determining the red fluorescence intensity of NPAFN (λex/λem = 488/650 nm) in the cells using confocal laser-scanning fluorescent microscopy (CLSM) and flow cytometry. The results in **Figure S5a** clearly indicate that the cells incubated with NPAFN-C18-PEG-MTX display more intense NPAFN fluorescence signal than those treated with NPAFN NPs and NPAFN-C18-PEG NPs due to the MTX's targeting ability. These findings can also be confirmed with a quantitative analysis by the flow cytometry results shown in **Figure S5b**.

Confocal imaging of cells was performed using a Leica laser scanning confocal microscope. Imaging of NPAPN (a kind of fluorescent probes) was carried out under 488 nm laser excitation and emission was collected in the range of 600 to 700 nm.

KB cells grown in FA (-) RPMI-1640 culture medium were seeded in 24-well plates (1 mL per well) incubated at 37 °C for 24 h. The cells were then incubated with the NPs and incubated for pre-determined time at 37 °C, and then washed twice with cold PBS, and digested by trypsin (0.05%)/EDTA treatment. The suspensions were centrifuged at 1000 rpm and 4 °C for 3 min. Then the supernatants were discarded and the cell pellets were washed with PBS to remove the background fluorescence in the medium. After two cycles of washing and centrifugation, cells were resuspended with 1 mL PBS and disrupted by sonication. The amount of NPAFN uptaken by KB cells was analyzed using the flow cytometry assay. A blank cell sample was measured as the control.

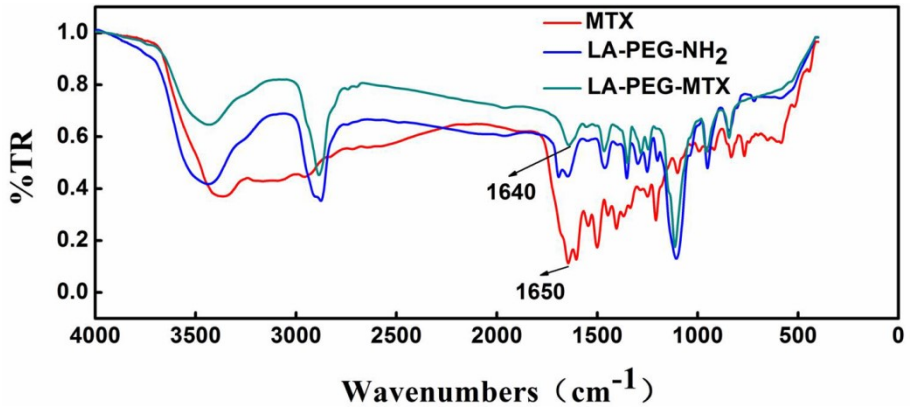

Figure S6. FTIR spectra of MTX, LA-PEG-NH_2 and LA-PEG-MTX.

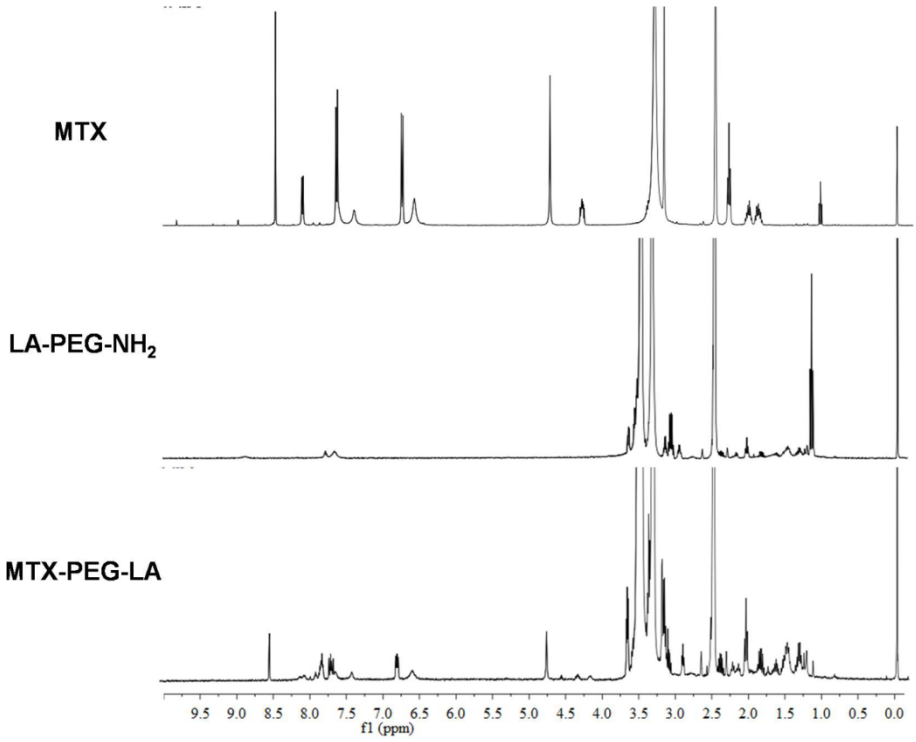

Figure S7. ^{1}H NMR spectra of MTX, LA-PEG-NH_2 and LA-PEG-MTX.

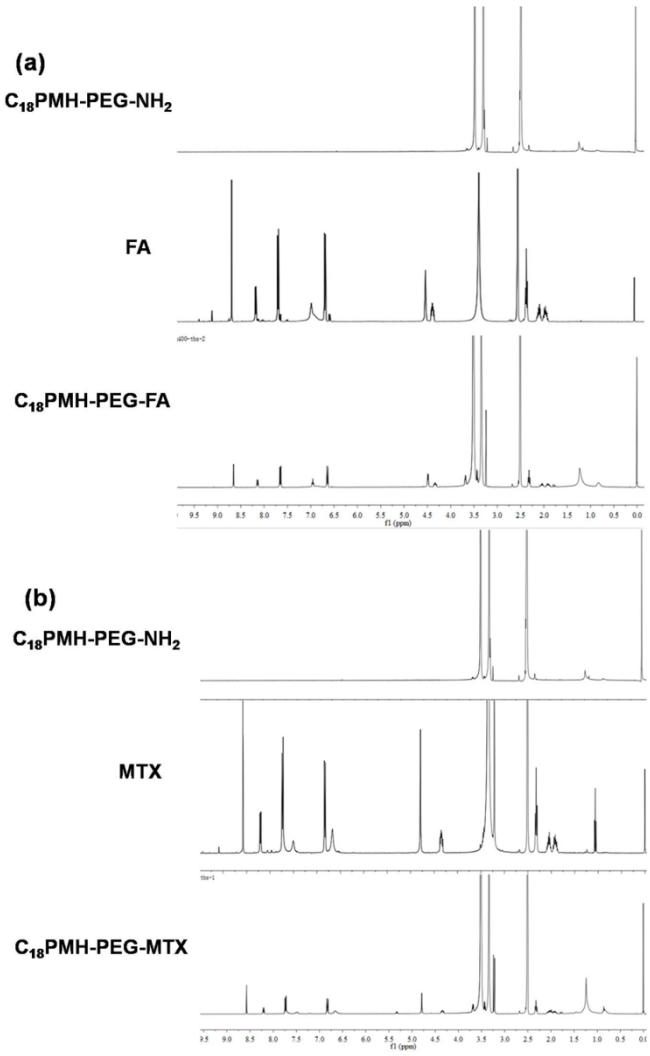

Figure S8. (a) ^{1}H NMR spectra of C18PMH-PEG-NH_2, FA, C18PMH-PEG-FA. (b) ^{1}H NMR spectra of C18PMH-PEG-NH_2, MTX, C18PMH-PEG-MTX.

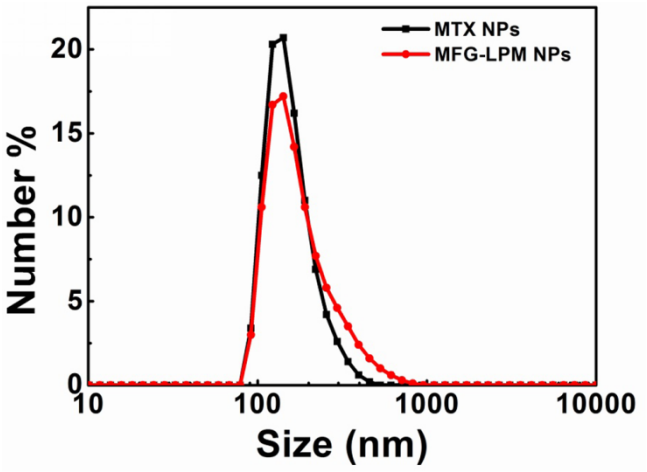

Figure S9. Size distribution of MTX NPs and MFG-LPM NPs by DLS measurements at 25 °C in water.

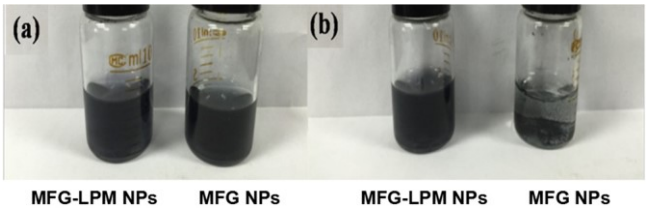

Figure S10. (a) Photographs of MFG-LPM NPs and MFG NPs immediate after preparation, and (b) at 3 days after preparation.

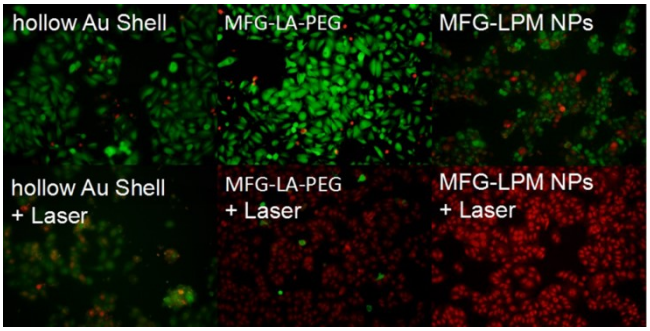

Figure S11. Fluorescence microscopy images of KB cells after being treated with hollow Au shell, MFG-LA-PEG NPs and MFG-LPM NPs under different conditions and co-stained with calcein AM and PI to indicate living and dead cells, respectively.

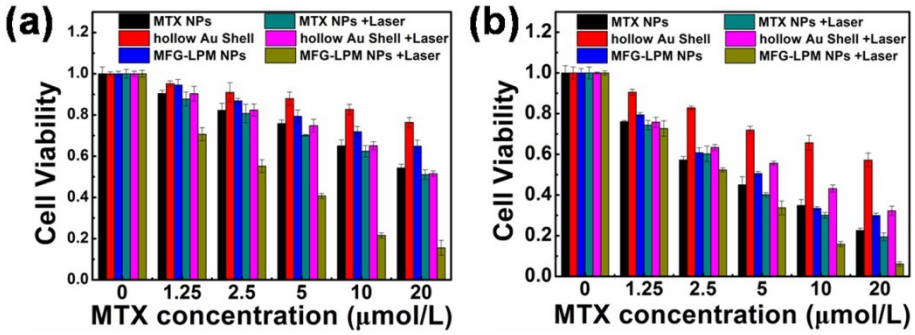

Figure S12. Cell viabilities of 4T1 cells treated with MTX NPs, hollow Au shell, MFG-LPM NPs, MTX NPs plus laser, hollow Au shell plus laser, and MFG-LPM NPs plus laser (λ = 808 nm, 1 W/cm^2, 10 min) for different periods including 24 h (a) and 72 h (b).

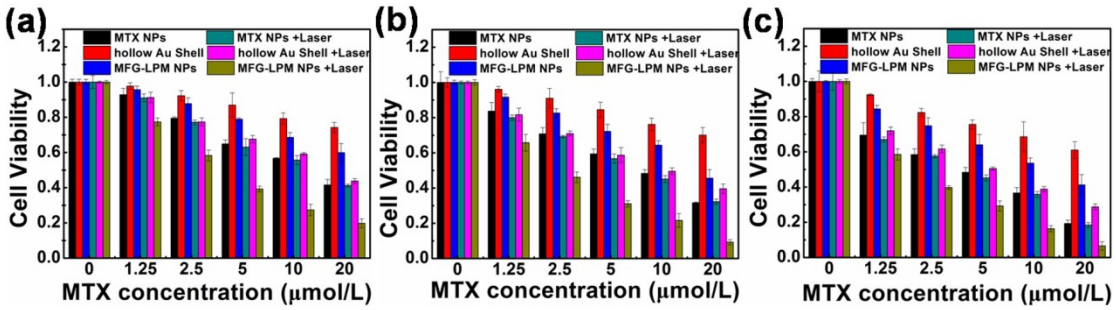

Figure S13. Cell viabilities of KB cells treated with MTX NPs, hollow Au shell, MFG-LPM NPs, MTX NPs plus laser, hollow Au shell plus laser, and MFG-LPM NPs plus laser (λ = 808 nm, 1 W/cm^2, 10 min) for different periods including 24 h (a), 48 h (b), and 72 h (c).

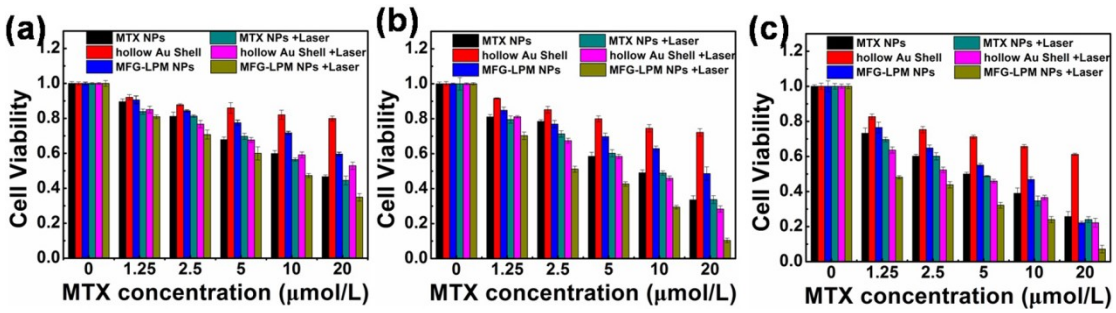

Figure S14. Cell viabilities of MRC-5 cells treated with MTX NPs, hollow Au shell, MFG-LPM NPs, MTX NPs plus laser, hollow Au shell plus laser, and MFG-LPM NPs plus laser (λ = 808 nm, 1 W/cm^2, 10 min) for various periods including 24 h (a), 48 h (b), and 72 h (c).

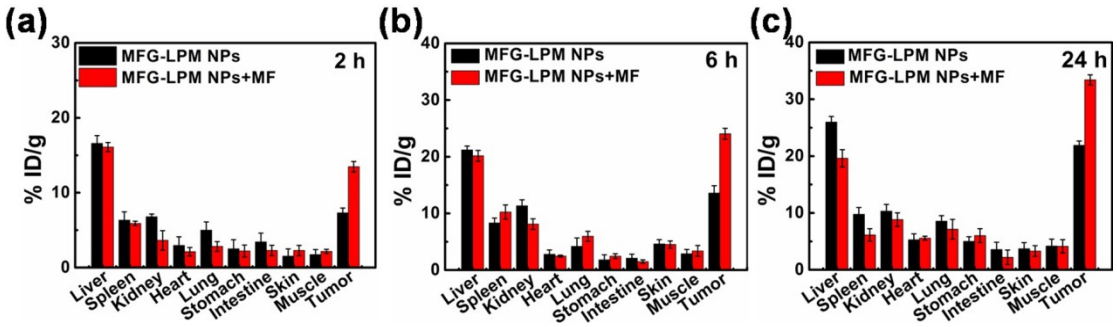

Figure S15. Biodistribution of MFG-LPM NPs in mice determined by the Au^{3+} from diluted tissue lysates for various periods including 2 h (a), 6 h (b), and 24 h (c).

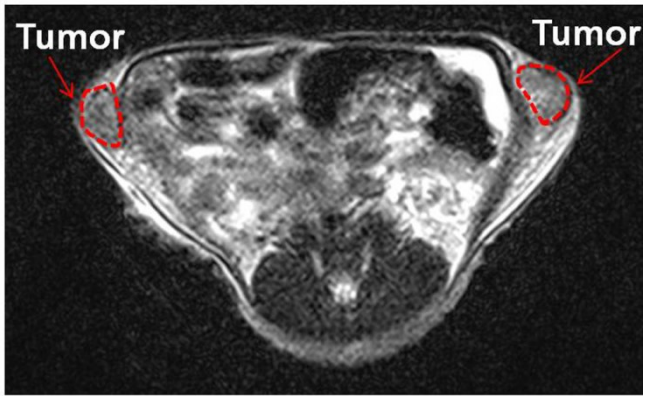

Figure S16. *In vivo* MR imaging of the two tumors on both left and right side at one day after intravenous injection of MFG-LPM NPs.